Planar hydraulic jump and associated hysteresis in near horizontal confined flow

Mrinmoy Dhar [1], Gargi Das [2,*] and Prasanta Kumar Das [1]
[1] *Department of Mechanical Engineering, Indian Institute of Technology, Kharagpur 721302, India*
[2] *Department of Chemical Engineering, Indian Institute of Technology, Kharagpur 721302, India*

(Received 18 December 2020; accepted 14 July 2021; published 5 August 2021)

Planar hydraulic jump at small inclinations of a narrow rectangular conduit is investigated by means of extensive experiments and theoretical analysis. Both upslope and downslope flows are considered for "natural" jumps formed solely by viscous shear without any geometrical obstruction. The effect of increasing conduit tilt from $-ve$ (upslope) to $+ve$ (downslope) is similar to increasing liquid flow rate. Additional intricacies are noted when flow downstream of the jump approaches the conduit ceiling. In particular, upslope flow exhibits unique instabilities and undergoes a hysteretic excursion to regain the initial stable state. The hydrodynamic states observed for different flow rate and conduit inclination are consolidated as a phase diagram that identifies the natural jump regime bounded by supercritical flow, subcritical flow, and full bore flow throughout the conduit and also demonstrates the existence of multiple hydrodynamic states for a certain range of operating conditions. This study reports jump induced hysteretic flow in sloping conduits. Apart from experiments, the classical shallow water theory is reformulated by incorporating the effect of turbulent viscosity and lateral averaging along the conduit width to account for sidewall effects. Additionally, mass and momentum balance across the jump is used to identify the domain of the natural jump in horizontal conduits. The theoretical predictions are in close agreement with experimental results. This is an analysis of the turbulent natural jump in slightly deviated narrow conduits.

DOI: 10.1103/PhysRevFluids.6.084803

I. INTRODUCTION

Liquid, during flow through a conduit, often undergoes an abrupt deceleration from supercritical to subcritical state; the transition is identified by change of Froude number Fr from greater than unity to less than 1. The visual manifestation of the deceleration is an abrupt elevation of free surface, termed "planar hydraulic jump" in fluid flow jargon. Planar jump of various forms is observed in nature and encountered in practical applications. For example, both stationary and traveling jumps are observed in rivers, canals, spillways, plumes, and partially filled conduits, and a submerged jump much below the free surface may occur in multilayer stratified flow. Due to their fascinating physics, jumps have attracted the attention of researchers since the last century but the majority of the studies address circular jumps or planar jumps in open channels. In-conduit hydraulic jumps have not received much attention and the few reported studies are for circular horizontal tubes.

One of the earliest studies in open channels was done by Lord Rayleigh [1] who described the jump as a shock. He proposed relations between the conjugate heights (free surface elevation before and after a jump under a particular flow condition) and the corresponding velocities from mass and momentum conservation considering inviscid flow upstream and downstream of the jump and

*gargi@che.iitkgp.ernet.in

also estimated energy loss across the jump. However, the inviscid flow theory failed to predict jump location. Subsequently, Watson [2] suggested a methodology to predict jump location for a known constant value of postjump height. Singha *et al.* [3] proposed a scaling relationship for jump location by vertical averaging of the stationary hydrodynamic equations. The analysis is based on the approach adopted by Bohr *et al.* [4] for circular hydraulic jumps. Bonn *et al.* [5] used shallow water theory to investigate planar jumps in narrow rectangular channels. In order to consider the substantial variation of velocity across flow, they performed lateral averaging in addition to vertical averaging, used commonly in shallow water theory.

For jumps inside a conduit [6–8], researchers have reported that the conduit shape as well as the free surface depth relative to the conduit diameter have a nontrivial influence, and a large enough postjump height may eventually cause a "choked flow" or "full conduit flow" [8]. Further, air above the liquid surface (either flowing or stationary) can get entrapped as the oscillating postjump liquid surface approaches the conduit top and causes slugging. Both full conduit flow and slugging substantially change the postjump hydrodynamics and can also influence the prejump flow behavior. Mortensen *et al.* [6] have further reported that the condition of gas and liquid entry and arrangement at the exit influence jump characteristics.

The past survey reveals that despite the interest in the planar hydraulic jump, there are several unresolved issues which obscure a proper understanding of the flow discontinuity. In particular, narrow, closed conduits, important in the current era of miniaturization, have received considerably less attention. It is expected that the flow physics will be more intriguing for slight deviations from the horizontal orientation, which is inevitable in practical situations. There are few studies in downsloped passages but all of them are for open channels [9–13] where the jumps were induced either by change in slope or by providing a sill. "Natural" hydraulic jumps due to viscous shear have rarely been considered [14]. Further, almost nothing is known about slightly deviated uphill flow even in open channels. Researchers have suggested jumps to be unstable except at high upstream Froude number; the limiting Fr is proposed as 9 and can be reduced to 4 by continuous adjustment of tail water level [15]. Pagliara and Peruginelli [16] suggested placement of a sill to stabilize jump on an upward slope while Baines and Whitehead [17] inferred that the jump is always unstable on an upward slope irrespective of the upstream Froude number and channel tilt. Later, based on momentum principle, Defina and Susin [18] concluded that a jump can be stable during uphill flow provided the channel wall friction is sufficiently high. This was verified experimentally by Defina *et al.* [19]. Dyment [20] generalized the approach proposed by Baines and Whitehead [17] and Defina and Susin [18] and formulated an approximate theoretical criterion for stability of stationary and moving jumps in an inclined conduit of arbitrary cross section.

In the present study, we focus on planar hydraulic jumps in narrow rectangular conduits, slightly inclined from the horizontal. Both upslope ($-ve$ inclination) and downslope ($+ve$ inclination) flows are considered for jumps formed solely by viscous action without any additional obstruction, referred to as "natural" jumps in the literature. The study comprises extensive experiments and theoretical analysis to understand the influence of conduit tilt and top wall confinement on the jump phenomena. The theoretical analysis modifies the shallow water equations by incorporating eddy viscosity in the momentum equations for supercritical and subcritical flow, and lateral averaging along with vertical averaging is executed to account for sidewall effects. In addition, the domain of the natural jump in horizontal conduits is identified from mass and momentum balance and validated with experimental observations. The experiments also identify jump stability and the flow phenomenon when the jump touches the conduit ceiling. Upslope flow exhibits a unique stable state, from which the conventional jump can be restored through hysteretic excursions. We summarize the observations as a phase diagram that illustrates the presence of multiple hydrodynamic states for identical input parameters. The presence of hysteresis in sloping conduits is reported in this study.

The organization of the paper is as follows. The experimental arrangement and results on jump formation and characteristics are discussed in Secs. II and III, respectively. The shallow water theory is reformulated in Sec. IV and the influence of top wall confinement is discussed in Sec. V. Section VI discusses experimental results on jump stability and the phenomena of hysteresis in upslope flow.

TABLE I. Flow variables in the test channels.

Conduit	h_{in} (mm)	Q ($\times 10^{-5}$ m^3/s) Min.	Q ($\times 10^{-5}$ m^3/s) Max.	Fr_{in} Min.	Fr_{in} Max.	$\mathrm{Re}_{in} = \mathrm{Re}\|_{Fr>1}$ Min.	$\mathrm{Re}_{in} = \mathrm{Re}\|_{Fr>1}$ Max.	$\mathrm{Re}\|_{Fr<1}$ Min.	$\mathrm{Re}\|_{Fr<1}$ Max.
A	1.1	2	26	14.59	189.71	1867	21666	450	6155
B	2.3	1.67	3.67	8.05	17.7	3112	6846	747	2324

Section VII consolidates the flow observations as a phase diagram and the salient conclusions of the study are summarized in section VIII.

II. EXPERIMENTAL ARRANGEMENT

The experiments are conducted in two narrow rectangular conduits for horizontal and slightly inclined orientation for both upslope ($-ve\ \theta$) and downslope ($+ve\ \theta$) flow. The conduits are 1720 mm in length and have a 0.24 aspect ratio (width, W_c/height, H_c). Conduit A is 12 mm wide and 50 mm high and conduit B is 6 mm wide and 25 mm high. In this paper, we primarily discuss the results for conduit A. Few results in conduit B are included to identify limiting conditions for the natural jump.

The conduit cross-sectional area is selected such that confinement by the side and top walls significantly influences the flow characteristics. It may be noted that the hydraulic jump depends not only on the conduit height H_c but also on its length L_c. Since the focus of the paper is to understand the effect of conduit inclination and confinement, we perform the experiments for a constant conduit length and ensure that the length is sufficient ($L_c = 1720$ mm) such that jumps form inside the conduit for a wide range of flow condition. We have discussed the effect of channel length on jump characteristics in one of our earlier studies on laminar natural jumps [14].

The conduit is mounted on leveling screws to align it perfectly horizontal and to change its tilt. The angle of inclination θ with the horizontal is varied from (–2.2°) to (+2.2°) in steps of 0.1° and is measured to a resolution of 0.05° by a digital inclinometer. The reproducibility of the results is examined by repeating the experiments several times.

Filtered tap water from a storage tank is supplied through an entry nozzle spanning the entire width of the conduit. The nozzle is always flush with the bottom wall of the test section even when the conduit is tilted. This arrangement facilitates a short flow development zone (approximately 50 mm from the inlet) where the liquid attains a uniform height along the conduit width. The section above the entry nozzle is closed and air cannot enter the conduit through the inlet. However, flow of air can occur at the outlet section. The conduit does not terminate abruptly; rather it ends in a smooth 90° bend with a 40 mm radius of curvature of the bottom surface. This allows the smooth exit of water during its free fall into the collecting tank, from where it is recirculated back to the entry of the test section. A schematic arrangement of the experimental facility is depicted in Fig. 1.

The flow parameters at the inlet, namely, liquid height h_{in}, water flow rate Q, Froude number Fr_{in}, and Reynolds number Re_{in} are listed in Table I for conduit A and B. The inlet Froude number is defined as $\mathrm{Fr}_{in} = V_{in}/\sqrt{gh_{in}\cos\theta} = q/\sqrt{gh_{in}{}^3\cos\theta}$ and the inlet Reynolds number is defined [5] as $\mathrm{Re}_{in} = h_{in}V_{in}/\nu = q/\nu$, where V_{in} is the inlet liquid velocity, q is the volume flow rate per unit width, g is the acceleration due to gravity, and ν is the kinematic viscosity. The volumetric flow rate Q is continuously metered by a Coriolis mass flowmeter (Micro Motion R050, range: 0–226.8 $\times$ 10^{-5} m^3/s, accuracy: ±0.5% of volume flow rate) and the accuracy of flow measurement is verified against volumetric measurement at the beginning of the experiments and between the test runs.

The range of Reynolds numbers for supercritical and subcritical flow in the two conduits is also listed in Table I. It may be noted that for supercritical flow prior to the jump, local liquid height

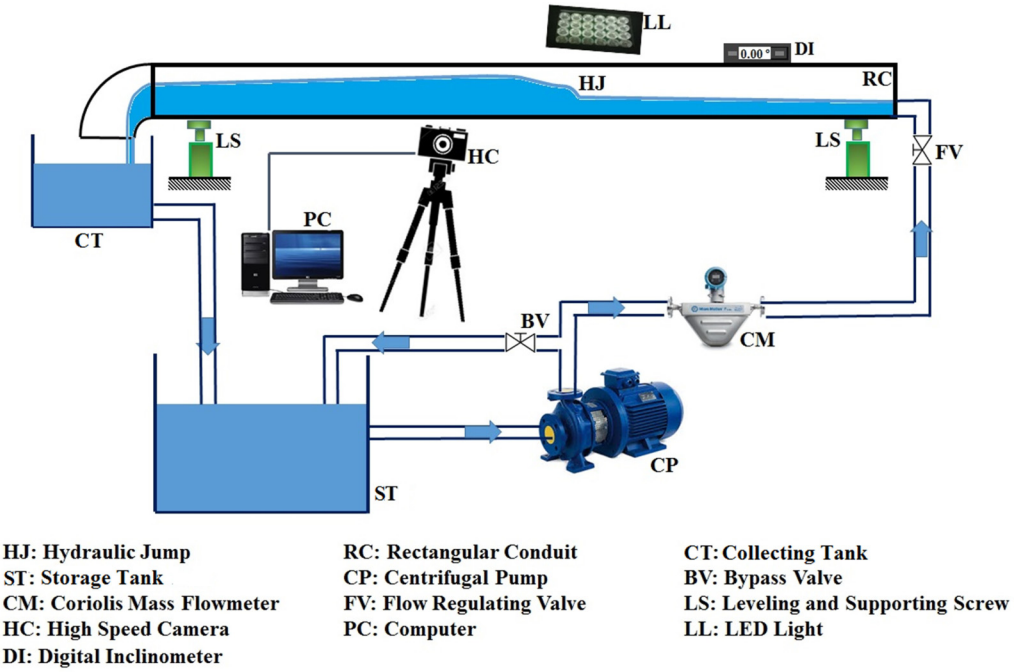

FIG. 1. Schematic of the experimental facility.

h is much smaller than the conduit width W_c, so the local Reynolds number for supercritical flow is defined in terms of h as $\mathrm{Re}|_{\mathrm{Fr}>1} = hV/\nu = q/\nu = \mathrm{Re}_{\mathrm{in}}$, where V is the local flow velocity. On the other hand, h typically is larger than W_c in the subcritical flow region after the jump and the local Reynolds number for subcritical flow $\mathrm{Re}|_{\mathrm{Fr}<1}$ is defined in terms of W_c as the characteristic length scale, viz., $\mathrm{Re}|_{\mathrm{Fr}<1} = W_c V/\nu = (W_c/h)(q/\nu) = (W_c/h)\mathrm{Re}_{\mathrm{in}}$. Thus the Reynolds number for supercritical flow is constant and equals the value at the inlet while after the jump, it varies with the local liquid height in the subcritical region.

The flow is predominantly along the axial direction and the flat walls of the rectangular conduit warrant minimum distortion to flow visualization. The details of free surface dynamics are captured from high-resolution video images recorded through the transparent (polyacrylic) sidewalls of the test sections. The axis of the camera is kept normal to the sidewalls and the images are recorded using a high-speed video camera [Phantom Miro LC-320S, M/S Vision Research, USA, speed: 1380 fps at full resolution (1920 × 1200) and 325 000 fps at minimum resolution (64 × 8)]. In order to ensure good quality images, the zone of interest is uniformly backlit with an LED panel. Most of the videos are recorded at 100 fps and 50 μs exposure time. Before each recording, sufficient time is provided for the readjustment of flow to the change in operating conditions, thus ensuring steady state conditions during the experiments. The color images [RGB, (red, green, blue)] extracted from the videos are converted into gray scale and subsequently into binary images. A code is developed in the MATLAB platform for estimating liquid height at different axial positions and jump location from the binary images.

III. JUMP PHENOMENON FROM FLOW VISUALIZATION STUDIES

Figure 2 presents a schematic of hydraulic jump in a tilted rectangular conduit. Conventionally, a jump is characterized by x_j, its location from the conduit entry, and strength, the ratio of conjugate free surface heights (h_2/h_1) where h_2 is the downstream elevation of free surface at a location where

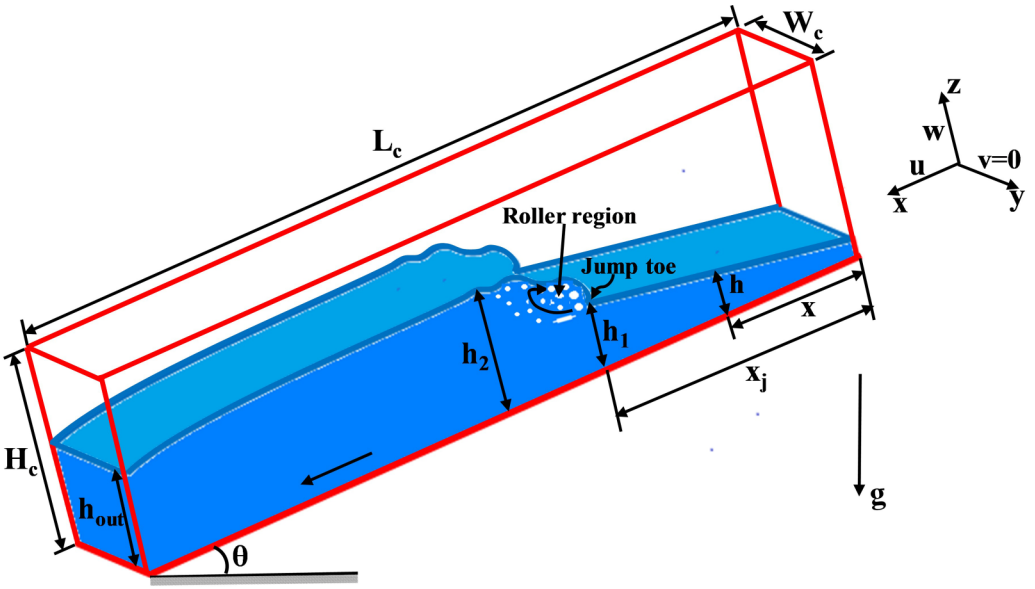

FIG. 2. Schematic of hydraulic jump in a narrow rectangular conduit inclined at θ to the horizontal.

the undulations have practically subsided and h_1 is the liquid height immediate upstream of jump, often referred to as "jump toe." At the jump region, we observe undulations at the free surface and small oscillations along the axial direction with a noticeable extent of air entrainment and eddy formation.

A. Jump types

Photographic images of a jump at $\theta = 0.2°, 0°$ (horizontal plane) and (–0.2°) are presented in Fig. 3(a) for identical input conditions, specified as dimensionless numbers for a generalized approach. Evidently, even a small slope alters the nature of the jump and there is striking difference between the jumps formed on upslope and downslope flow. This is an expected outcome as in

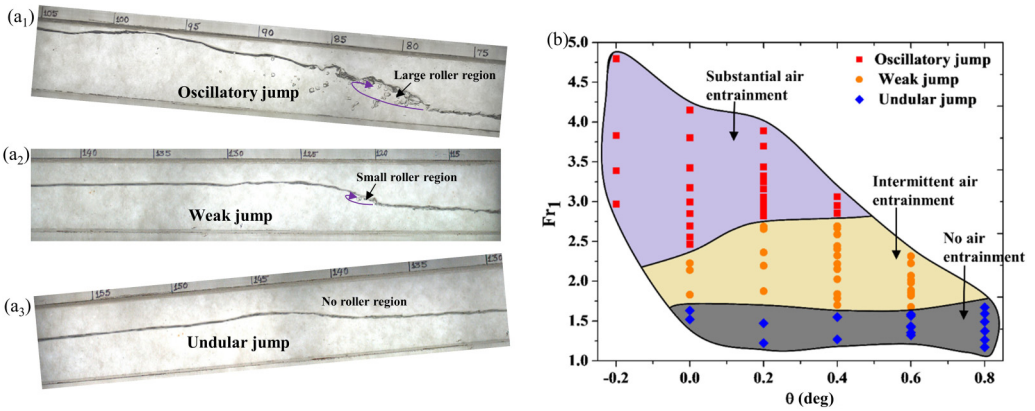

FIG. 3. (a) Effect of inclination on the nature of a jump at $\mathrm{Fr_{in}} = 118.37$ and $\mathrm{Re_{in}} = 15\,558$. ($a_1$)–($a_3$) display oscillatory jump in upslope flow ($\theta = -0.2°$), weak jump in horizontal flow ($\theta = 0°$), and undular jump in downslope flow ($\theta = 0.2°$). (b) Phase diagram depicting the jump types in the ($\mathrm{Fr_1} - \theta$) plane.

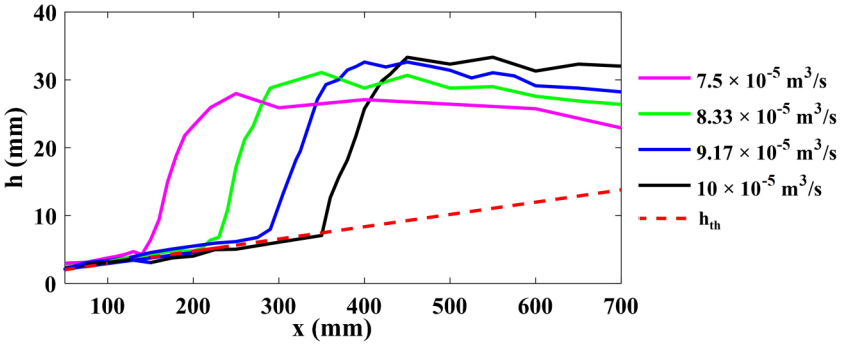

FIG. 4. Experimental free surface profiles (solid lines) at different Q for $\theta = 0^\circ$ vis-à-vis theoretical prediction [h_{th}: Eq. (1)], shown by dashed line with $k = 0.1$.

a horizontal plane, gravity merely affects the local hydrostatic head while for inclined conduits, gravity either opposes flow or assists it.

From visualization studies in the experimental domain ($1867 \leqslant \text{Re}_{\text{in}} \leqslant 21\,666$, $-2.2^\circ \leqslant \theta \leqslant 2.2^\circ$), we observe jump characteristics similar to those reported for wide channels [9]. Following the nomenclature used for wide channels, jumps are classified as oscillatory, weak, and undular based on visual appearance, and the classification is further quantified on the basis of jump strength h_2/h_1 as obtained from the present experiments. An undular jump exhibits an undulating liquid surface without any air entrainment and roller region, and is characterized by $1 < h_2/h_1 \leqslant 1.75$ while a weak jump identified by a smooth rise in liquid level with intermittent air entrainment and small roller region is identified by $1.75 < h_2/h_1 \leqslant 2.5$. On the other hand, an oscillatory jump associated with significant air entrainment, large roller region, and instability of high-velocity flow exhibits jump strength in the range $2.5 < h_2/h_1 \leqslant 5$. This kind of jump oscillates in a random manner, giving rise to large surface waves that propagate over a substantial distance downstream. Figure 3(a) presents snapshots of the three types and Fig. 3(b) presents their range of existence in the $\text{Fr}_1 - \theta$ plane where Fr_1 refers to the immediate upstream Froude number. For conduits inclined at θ to the horizontal, the local Froude number Fr is defined as $\text{Fr} = V/\sqrt{gh\cos\theta} = q/\sqrt{gh^3\cos\theta}$. From Fig. 3(b), the jump type is noted to be significantly influenced by Fr_1, irrespective of conduit tilt and a particular type of jump occurs for more or less the same range of Fr_1 over the experimental range of $+ve$ and $-ve$ θ.

Oscillatory jump [Fig. 3(a_1)] formed at higher Fr_1 is associated with large void formation and substantial air entrainment at the jump toe, while a weak jump [Fig. 3(a_2)], occurring at a lower magnitude of relative velocity between the incoming supercritical flow and the roller region, exhibits reduced void formation with limited number of air bubbles entrained in an irregular fashion. During undular jump [Fig. 3(a_3)], air entrainment diminishes drastically and the flow discontinuity is not associated with void formation. In general, oscillatory nature and air entrainment increase with an immediate upstream Froude number for the operating range considered in the present work.

B. Free surface profiles and jump parameters

The free surface profiles are presented in Figs. 4–6 for horizontal, adverse inclination (upslope), and positive (downslope) inclination respectively. In the figures, h is the height of the liquid layer at a distance x from the entry. For all conduit inclinations, the jump location shifts downstream with increase in flow rate as expected and the liquid height gradually increases in supercritical flow upstream of the jump. This is clearly an effect of viscosity.

Figure 4 shows h to be a linear function of axial distance independent of flow rate. The same has also been reported by Bonn *et al.* [5] who have proposed the prejump height profile in horizontal

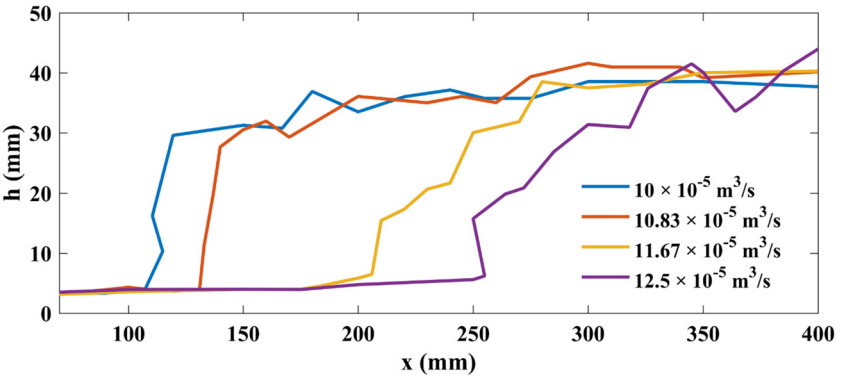

FIG. 5. Experimental free surface profiles for different Q at $\theta = -0.2^\circ$.

flow as

$$h \approx 1.81k^2(x - x_0), \tag{1}$$

where x_0 is the axial position at $h = 0$, obtained by extrapolating the experimental height profiles to zero. From the present experiments, the constant $k = 0.1$ and $x_0 = -61.94$ mm. The fitting of Eq. (1) thus satisfies the experimentally estimated height of the water layer over the entire supercritical flow region (Fig. 4) from the entry to the jump region.

An identical trend is observed for upslope flows in Fig. 5 where the prejump height profiles are more or less linear and collapse to a single curve. On the other hand, for downslope flow (Fig. 6), the upstream profiles, although approximately linear, do not converge to a single curve as the profiles are steeper at lower water flow rate.

From the experimentally obtained free surface profiles, the jump location (scaled with respect to immediate upstream liquid height) and strength are estimated and presented as a function of inlet Reynolds number $\mathrm{Re_{in}}$ and θ in Figs. 7(a) and 7(b), respectively. The figures show that increasing θ has the same effect as increasing $\mathrm{Re_{in}}$ although they counter shear by different means. Liquid inertia becomes important at higher $\mathrm{Re_{in}}$ while gravity governs the orientation effect.

Compared to a horizontal conduit, a jump moves closer to the inlet in upslope flow and in the opposite direction for downslope conduits. Jump strength also decreases as the conduit tilt is shifted from $-ve$ to $+ve$ slope at constant liquid flow. The rapid decrease is due to a simultaneous increase

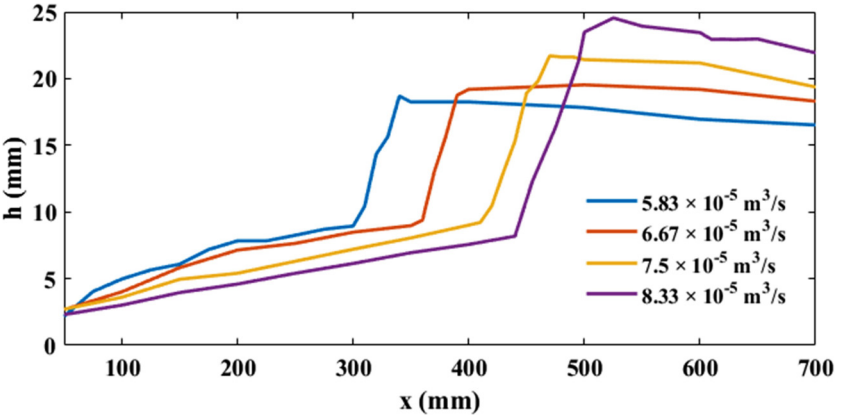

FIG. 6. Experimental free surface profiles for different Q at $\theta = 0.5^\circ$.

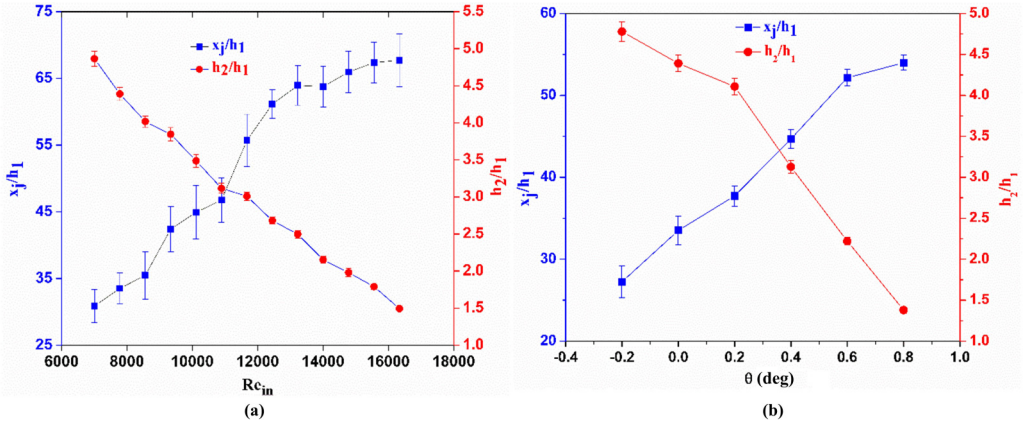

FIG. 7. Scaled jump location and jump strength as function of (a) $\mathrm{Re_{in}}$ at $\theta = 0^\circ$ and (b) θ at $\mathrm{Re_{in}} = 7780$.

in h_1 and decrease in h_2 with increase in slope. This is accompanied by a decrease in both oscillations and quantity of air entrained into the roller region. Thus, oscillation and air entrainment have a strong mutual interplay and a higher jump strength is conducive for both.

Interestingly Fig. 8 shows that data points pertaining to a particular jump type in a horizontal conduit cluster together when presented in the $h_2/h_1 - \mathrm{Fr}_1$ plane and a consistent linear variation of jump strength with Fr_1 is exhibited irrespective of jump type and extent of air entrainment (Fig. 8). This is similar to the results reported in wide horizontal channels. The past researchers [21,22] have expressed jump strength as function of upstream Froude number from a modified form of classical jump equation (Bélanger equation [9]):

$$\frac{h_2}{h_1} = \frac{-1 + \sqrt{1 + 8\chi \mathrm{Fr}_1^2}}{2}. \tag{2}$$

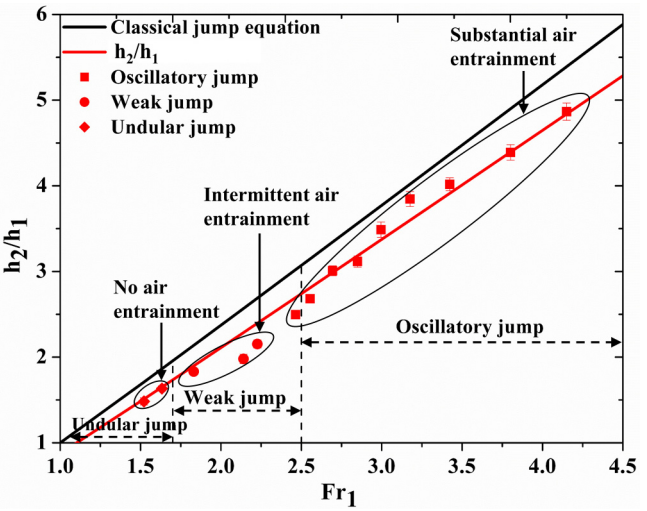

FIG. 8. Jump strength, air entrainment, and jump type as function of Fr_1. Black and red lines represent the classical jump equation and the modified version [h_2/h_1: Eq. (2)], respectively. Data points represent experimental results.

The equation incorporates a constant χ to improve predictions. Several values for χ have been proposed in the literature based on phenomenological arguments and experimental results [22]. However, a universally accepted value is still missing. In Fig. 8, the classical Bélanger equation shown by a black solid line overpredicts jump strength, irrespective of jump type, and from linear regression, we obtain $\chi = 0.82$ with $R^2 = 0.98$.

IV. SHALLOW WATER ANALYSIS

Shallow water equations [14,23] are formulated to predict the free surface profiles upstream and downstream of a jump, based on which the jump location is identified in narrow, rectangular conduits, slightly deviated from the horizontal. The formulation is based on the following considerations.

(1) Axial momentum dissipation is negligible compared to transverse momentum dissipation (along the z axis).

(2) The height of the liquid layer is much less compared to the axial length scale, so velocity variation across liquid height is incorporated by averaging, similar to the analysis of boundary layer (or thin film) flow. Although this assumption is not true particularly in the postjump region, reasonably good agreement is obtained with experimental results for jumps of various types [5,14,23].

(3) The effect of gravity is incorporated by hydrostatic pressure approximation.

(4) Two-dimensionality of flow is violated due to the presence of sidewalls, so lateral averaging along the channel width is performed, following the methodology of Bonn *et al.* [5].

(5) Significant flow turbulence is present due to the high frictional forces and strong mixing induced by confinement of the closely spaced conduit walls. This is incorporated by using turbulent eddy viscosity ν_t instead of the kinematic viscosity of the liquid, and is based on the observations of Bonn *et al.* [5] that the local free surface height is an order of magnitude higher compared to the predictions from laminar flow with a comparable Reynolds number. This is more relevant in the present study as the Reynolds number range is higher in our experiments and is further confirmed by the linear and flow rate independent free surface profiles prior to a jump, similar to that reported by Bonn *et al.* [5]. Accordingly, a direct proportionality between Prandtl's mixing length and the smallest length scale of flow is assumed, viz., $\nu_t \approx k^2 q$.

Following the nomenclature specified in Fig. 2, the local continuity equation for steady state flow of an incompressible fluid in a planar geometry is

$$\frac{\partial u}{\partial x} + \frac{\partial w}{\partial z} = 0, \tag{3}$$

and the momentum equation, assuming eddy viscosity to be the sole contributor to shear stress, is

$$u\frac{\partial u}{\partial x} + w\frac{\partial u}{\partial z} = -g\cos\theta\frac{dh}{dx} + \nu_t\left(\frac{\partial^2 u}{\partial y^2} + \frac{\partial^2 u}{\partial z^2}\right) \pm g\sin\theta. \tag{4}$$

Further, the condition for constant volume flux gives

$$Q = \int_0^h dz \int_0^{W_c} dy u(x, y, z), \tag{5}$$

where the x, y, and z axes refer to the direction of flow, the direction along the conduit width (W_c), and the vertical upward direction, respectively (Fig. 2), and the x component of velocity u and the z component of velocity w have a spatial dependence of the form $u = u(x, y, z)$ and $w = w(x, y, z)$. Liquid does not flow along the conduit width ($v = 0$) and the liquid height also does not vary along the y axis. From the adopted sign convention, $g\sin\theta$ is $+ve$ for downslope flow and $-ve$ for upslope cases.

Assuming no-slip and no-penetration boundary conditions at the bottom and sidewalls and no shear stress at the free surface, $u(x,\ y,\ 0) = w(x,\ y,\ 0) = 0,\ u(x,\ 0,\ z) = w(x,\ 0,\ z) = 0,$ $u(x,\ W_c,\ z) = w(x,\ W_c,\ z) = 0$, and $\frac{\partial u}{\partial z}|_{z=h(x)} = 0$.

Considering separable and self-similar velocity profile, $u(x, y, z) = V(x)e(\xi)f(\eta)$, where V is the average velocity; $\xi = \frac{y}{W_c}, 0 \leqslant \xi \leqslant 1$, and $\eta = \frac{z}{h(x)}, 0 \leqslant \eta \leqslant 1$.

The profile satisfies $e(0) = 0\ e(1) = 0,\ f(0) = 0,\ f'(1) = 0, \int_0^1 e(\xi)d\xi = \int_0^1 f(\eta)d\eta = 1$.

Based on this, a simple and physically reasonable parabolic velocity profile has been considered, viz., $e(\xi) = 6\,\xi\,(1 - \xi)$ and $f(\eta) = 3\eta - \frac{3}{2}\eta^2$.

Using the continuity equation and averaging the momentum equation in the y direction, the following equation is obtained,

$$\beta_1\left(u\frac{\partial u}{\partial x} + w\frac{\partial u}{\partial z}\right) = -g\cos\theta\frac{dh}{dx} - \nu_t\left(\frac{cu}{{W_c}^2} - \frac{\partial^2 u}{\partial z^2}\right) \pm g\sin\theta, \tag{6}$$

where u and w are averaged over the y direction and $\beta_1 = \int_0^1 e^2(\xi)d\xi$ and $c = -2\frac{de}{d\xi}|_{\xi=1}$.

For the parabolic profile considered, β_1 and c are obtained as constants with $\beta_1 = \frac{6}{5} = K_1$ and $c = 12$. Integrating the momentum equation in the z direction and using the continuity equation and the boundary conditions, the following equation is obtained,

$$\beta_1\frac{1}{h}\frac{d}{dx}\int_0^h u^2 dz = -g\cos\theta\frac{dh}{dx} - \nu_t\left(\frac{cV}{{W_c}^2} + \frac{1}{h}\frac{\partial u}{\partial z}\bigg|_{z=0}\right) \pm g\sin\theta, \tag{7}$$

which can be reduced to

$$\beta_1\beta_2 V\frac{dV}{dx} = -g\cos\theta\frac{dh}{dx} - \nu_t\left(\frac{cV}{{W_c}^2} + \frac{1}{h}\frac{\partial u}{\partial z}\bigg|_{z=0}\right) \pm g\sin\theta, \tag{8}$$

where $\beta_2 = \int_0^1 f^2(\eta)\,d\eta$.

For the assumed velocity profile, β_2 is constant and is equal to $\frac{6}{5} = K_2$, and $\frac{\partial u}{\partial z}|_{z=0} = \frac{3V}{h} = \frac{K_3 V}{h}$ where K_3 (similar to K_1 and K_2) depends on the velocity profile.

Hence, the equation for the height profile becomes

$$K_1K_2\frac{q^2}{h^3}\frac{dh}{dx} = g\cos\theta\frac{dh}{dx} + \nu_t\left(\frac{cq}{{W_c}^2 h} + \frac{K_3 q}{h^3}\right) \mp g\sin\theta. \tag{9}$$

The above equation is now rescaled with the use of the critical height $h_{\text{crit}} = (K_1K_2)^{1/3}q^{2/3}(g\cos\theta)^{-1/3}$. From order of magnitude analysis, we obtain

$$h = h_{\text{crit}}H = (K_1K_2)^{1/3}q^{2/3}(g\cos\theta)^{-1/3}H, \tag{10a}$$

$$x = K_1K_2{K_3}^{-1}k^{-2}h_{\text{crit}}X = (K_1K_2)^{4/3}{K_3}^{-1}k^{-2}q^{2/3}(g\cos\theta)^{-1/3}X. \tag{10b}$$

In the supercritical flow region, the smallest length scale is liquid height h. This transforms Eq. (9) to a general form

$$(1 - H^3)\frac{dH}{dX} = 1 + DH^2 \mp EH^3, \tag{11}$$

where $D = (K_1K_2)^{2/3}{K_3}^{-1}q^{4/3}(g\cos\theta)^{-2/3}{W_c}^{-2}c$ and $E = K_1K_2{K_3}^{-1}k^{-2}\tan\theta$.

Equation (11) is valid for the supercritical flow region as long as the liquid height h is the smallest length scale; i.e., $h < \mathrm{W}_c$.

In the subcritical flow region, h is typically larger than W_c and it is reasonable to assume mixing length proportional to W_c instead of h; i.e., $l_m = k_y W_c$ (assuming $k_y = k$). The turbulent eddy

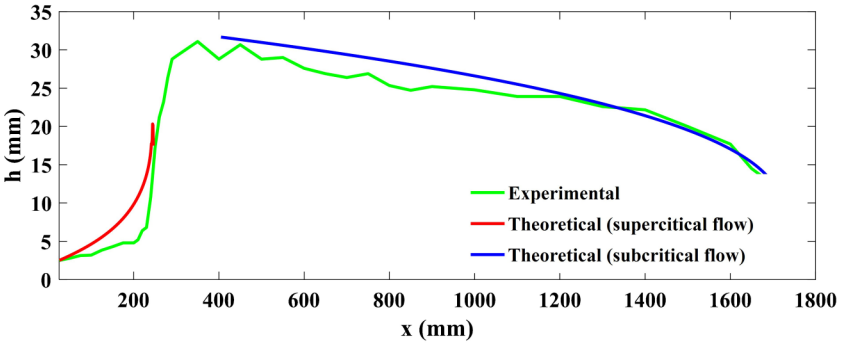

(a)

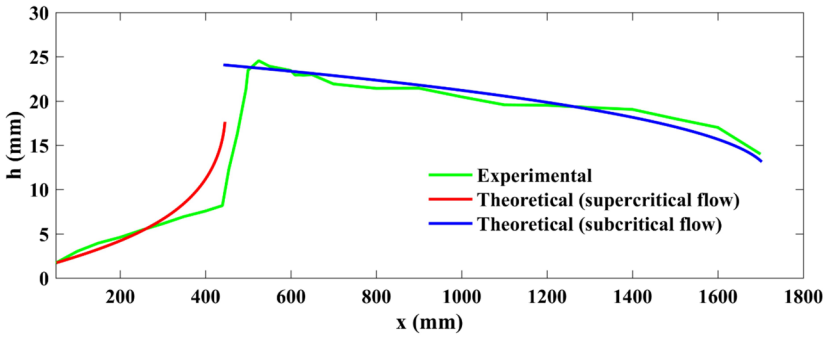

(b)

FIG. 9. Experimental and theoretical free surface profiles in the supercritical and subcritical flow region for $\mathrm{Fr_{in}} = 59.18$, $\mathrm{Re_{in}} = 7780$, and (a) $\theta = 0^\circ$ and (b) $\theta = 0.5^\circ$. For the theoretical profiles we use $k \approx 0.1$ and $h_r = 0.5$ in (a) and $k \approx 0.08$ and $h_r = 0.6$ in (b).

viscosity in the subcritical region thus becomes $\nu_{t,\,\mathrm{subcritical}} = k^2 q \frac{W_c}{h}$, which changes Eq. (11) as

$$(1 - H^3)\frac{dH}{dX} = \frac{1}{H}(1 + DH^2 \mp EH^3). \tag{12}$$

Here, the scale for h retains the same form as Eq. (10a) and the axial scale changes as $x = (K_1 K_2)^{4/3} K_3{}^{-1} k^{-2} q^{4/3} (g\cos\theta)^{-2/3} W_c{}^{-1} X$.

We use a fourth-order Runge-Kutta method for numerical solution of Eqs. (11) and (12) for supercritical and subcritical flow region, respectively. The supercritical flow solution upstream of a jump depends on the upstream boundary condition and the liquid height increases with the progress of flow in the forward direction until it attains a critical height ($H = 1$) where the solution becomes discontinuous. Taking cue from the literature [3,14,23,24] we treat this discontinuity as a hydraulic jump and postulate the jump to lie in the vicinity of this discontinuity.

The subcritical flow solution downstream of the jump is obtained by using the boundary condition at the outlet. Taking a cue from Dhar *et al.* [14,23,25], we consider the outlet liquid height to be critical ($h_{\mathrm{out}} = h_{\mathrm{crit}}$) and start our solution slightly before the conduit exit to proceed in the negative x direction. This consideration is not arbitrary and can be supported by energy balance at the outlet flow condition.

Typical representative results are presented in Figs. 9(a), 9(b), and 10 for horizontal, downslope, and upslope flow, respectively. The input parameters in the figures are specified as dimensionless parameters to facilitate a generalized approach for interpretation of results. The free surface profiles

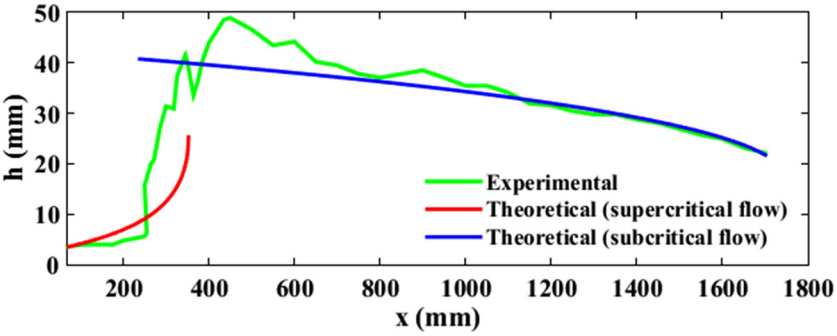

FIG. 10. Experimental and theoretical free surface profiles in the supercritical and subcritical flow region for $\mathrm{Fr_{in}} = 88.77$, $\mathrm{Re_{in}} = 11\,669$ and $\theta = -0.2^\circ$. For the theoretical profiles we use $k \approx 0.085$ and $h_r = 0.7$.

in a horizontal conduit [Fig. 9(a) for $\mathrm{Fr_{in}} = 59.18$ and $\mathrm{Re_{in}} = 7780$] can be predicted from the generalized model as a special case by substituting $\theta = 0^\circ$ and $E = 0$. The constant k is obtained as 0.1 from experimental results (Fig. 4). The solution of Eq. (11) depicted by the lower branch in Fig. 9(a) becomes discontinuous at $H = 1$. A comparison with the experimentally obtained profile superimposed in the same figure indicates that the jump is located very close to this discontinuity position. Further, the qualitative trends predicted from theory matches well with the experimental profiles both upstream and downstream of the jump and the theoretically predicted free surface profile in the supercritical region lies close to the experimental curve.

A similar trend is also noted in inclined conduits. This is evident from Figs. 9(b) and 10 which present the theoretical and experimental free surface profiles for $\theta = 0.5^\circ$ and $\theta = -0.2^\circ$, respectively. Both figures display good agreement between the experimentally estimated and the theoretically predicted jump locations and the upstream profiles.

The k values computed from the experimental results for both upslope and downslope flows present an interesting trend. While for upslope flow (Fig. 10), the k value is close to 0.08 over the range of inclination considered ($\theta \leqslant -0.2^\circ$), it appears to be a weak function of conduit tilt for downslope flow. As shown in Fig. 9(b), the value is $k \approx 0.08$ for $\theta = 0.5^\circ$. We further note that k is not a function of flow rate for horizontal and upslope conduit but depends on flow rate for downslope flow. This can be attributed to our experimental observation (Figs. 4 –6) which reveals the upstream free surface profiles to be independent of flow rate for the horizontal and upslope orientation while being a significant function of flow rate in downward sloping conduits. In any case, the value of k for the entire range of conduit inclination is close to 0.1, the value obtained in a horizontal conduit.

The figures further reveal that the theoretically obtained solution of Eq. (12) consistently overpredicts the experimental results in the subcritical flow region. The discrepancy arises as the experimentally measured liquid height at the outlet (h_{out}) is lower than h_{crit}. This is an anticipated outcome considering the inherent simplicity of the model compared to the actual flow situation. In reality, the flow involves turbulent mixing, intense surface fluctuations at the jump region, air entrainment into the liquid, and air entrapment between the liquid surface and the confining walls, while the model considers turbulence by the mere inclusion of eddy viscosity instead of kinematic viscosity of the fluid. Additionally, the appreciable curvature of the free surface where the liquid falls freely from the conduit also results in nonhydrostatic pressure distribution at the exit. In order to improve the predictions, we tune the height at the outlet in light of our experimental estimations which show that the liquid height at the exit is only a fraction of the critical height in the supercritical flow region. We thus incorporate a tuning factor h_r which is the ratio of critical height in subcritical flow to the critical height predicted from supercritical flow solution. A similar adjustment of liquid height at the exit was also adopted by Bonn *et al.* [5]. For a horizontal conduit, we obtain improved

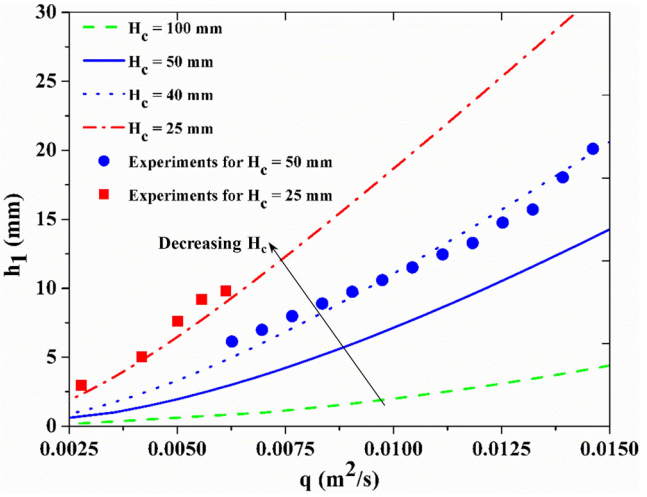

FIG. 11. Variation of upstream height with flow rate per unit width for different conduit heights. Curves represent Eq. (14) and circles and squares denote experimental results in conduits A and B, respectively.

predictions for $h_r = 0.5$ and in inclined conduits, the value is always close to 0.5. Figures 9(b) and 10 show improved predictions in the subcritical flow region with $h_r = 0.6$ and 0.7, respectively.

The incorporation of fitting parameters k and h_r is necessary as the present theory is based on several simplifying assumptions. Further, the influence of certain factors such as intense surface fluctuation and air entrainment into the liquid cannot be accounted for under the paradigm of the present modeling approach. The air entrapped between the liquid surface and confining walls also imposes a unique effect on the flow hydrodynamics. Each of these factors depends on the phase flow rate as well as the conduit tilt and thus affects the outlet height. With the present methodology, it is not possible to predict generalized functions for these fitting parameters, so these are obtained from experimental data for specific flow conditions. Nevertheless, the values in inclined conduits are close to the values obtained for the horizontal conduit. For a more accurate estimation without inclusion of fitting parameters, one needs to resort to a higher-order numerical tool, mostly, a computational fluid dynamics (CFD) algorithm, to capture all the relevant hydrodynamic parameters.

V. TOP WALL CONFINEMENT

Evidently, a natural hydraulic jump in a closed conduit can occur only when the free surface elevation after the jump h_2 is less than the conduit height H_c. In a horizontal conduit, this limiting condition can be estimated from mass and momentum balance across the jump.

Assuming free surface flow of an ideal fluid, this gives

$$h_1 h_2 (h_1 + h_2) = \frac{2q^2}{g}, \tag{13}$$

where substituting $h_2 = H_c$ and neglecting the physically meaningless solution, we get

$$h_1 = \frac{H_c}{2}\left(\sqrt{1 + \frac{8q^2}{gH_c^3}} - 1\right). \tag{14}$$

The equation suggests that the limiting condition is decided by the coupled effect of upstream liquid level and flow rate per unit width (q). The graphical relationship between the two parameters is displayed in Fig. 11 for different conduit heights. As dictated by Eq. (14), the curves are closer

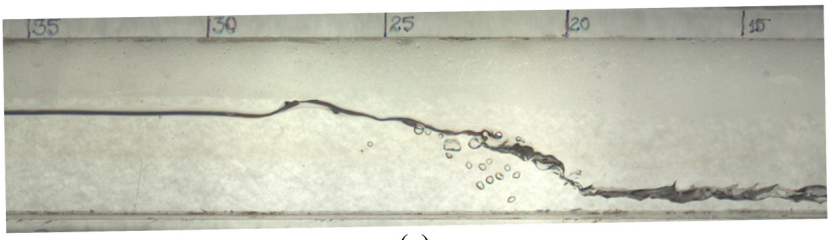

(a)

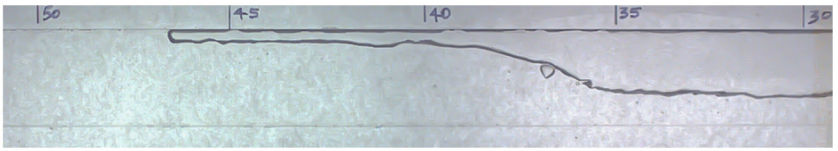

(b)

FIG. 12. Free surface profile in conduit A and B at $q = 0.006\,\mathrm{m}^2/\mathrm{s}$, (a) $h_1 = 9.82\,\mathrm{mm}$, $H_c = 50\,\mathrm{mm}$, and (b) $h_1 = 7.63\,\mathrm{mm}$, $H_c = 25\,\mathrm{mm}$.

to the abscissa for higher values of H_c. The experimental data for conduits A ($H_c = 50\,\mathrm{mm}$) and B ($H_c = 25\,\mathrm{mm}$) are included in Fig. 11 to enable a comparative study.

From the experiments, we observe that the limiting jump condition is attained in the smaller conduit while a natural jump occurs over the entire range in conduit A. The same is displayed in Fig. 11 where the experimental data denoted by "blue circles" (conduit A) lie closer to the curve for $H_c = 40\,\mathrm{mm}$ (dotted blue) rather than the curve for $H_c = 50\,\mathrm{mm}$ (solid) while the proximity of the squares to the $H_c = 25\,\mathrm{mm}$ (dashed-dot) curve clearly indicates that liquid downstream of the jump touches the conduit ceiling in the smaller conduit. Photographs for a representative flow condition ($q = 0.006\,\mathrm{m}^2/\mathrm{s}$) in conduit B (Fig. 12) validate the conjecture. At $q = 0.006\,\mathrm{m}^2/\mathrm{s}$, the corresponding $h_1 = 9.82\,\mathrm{mm}$ in conduit A and 7.63 mm in conduit B. Considering ideal fluid flow, the postjump height from the Bélanger equation is 33.02 mm in conduit A and 22.99 mm in conduit B. This again confirms sufficient clearance between postjump liquid surface and conduit ceiling in the former case and a marginal clearance in the smaller conduit. Thus Eq. (14) presented as Fig. 11 can be used to identify confinement effects due to the presence of the top wall.

As the jump in conduit B [Fig. 12(b)] touches the top wall within some distance from its inception, full bore flow takes place. This is often accompanied by intermittent air entrainment close to the conduit ceiling and free surface oscillations reaching the top as a large wave. The waves form a bridge, which entraps the stagnant air and pushes it away from the jump. The phenomenon, depicted by a sequence of images in Fig. 13, resembles slugging, well reported for gas-liquid flow. In the present experiments, slugging is induced during only liquid flow by top wall confinement.

We further attempt to verify whether the conduit ceiling influences jump even when the free surface is much below it. For this, we repeat a few experiments by removing the top wall of conduit A. No noticeable difference in flow behavior is observed. This confirms that the confinement effect plays a crucial role only when the jump can graze against the ceiling and equations well established for open channel flow can be used to predict the hydrodynamics in closed conduits for $H_c > h_2$.

The same is also verified by testing if the theoretical criterion for jump stability in upslope wide channel flow [18,19] holds true for narrow closed conduits.

$$\frac{C^2 \tan\theta}{g} > -2\mathrm{Fr}_1^2 \frac{\sqrt{1+8\mathrm{Fr}_1^2}+1}{\left(\sqrt{1+8\mathrm{Fr}_1^2}-1\right)^2}, \tag{15}$$

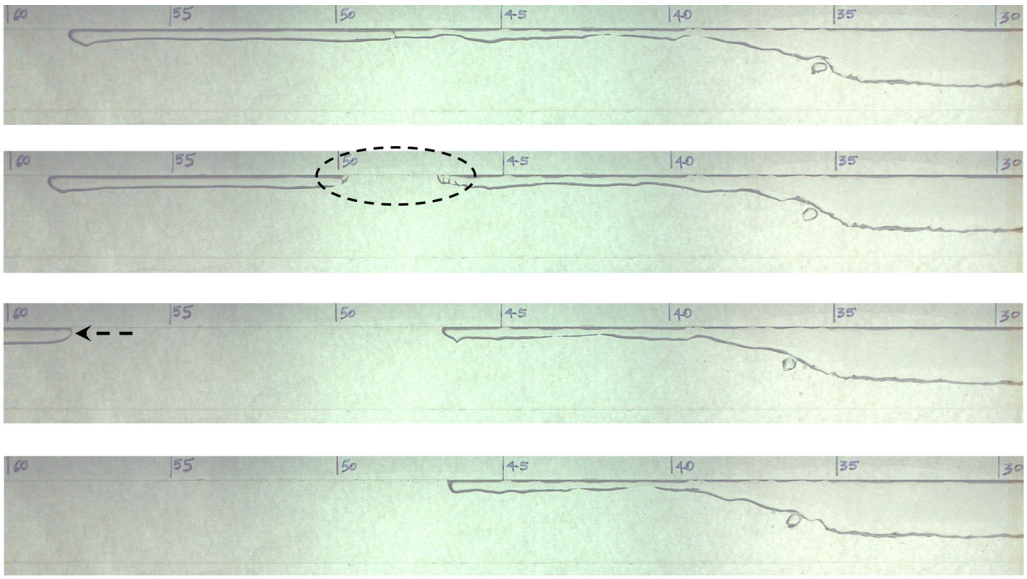

FIG. 13. Sequence of images depicting slugging; $q = 0.006\,\mathrm{m}^2/\mathrm{s}$, $H_c = 25\,\mathrm{mm}$.

The criterion [Eq. (15)] is based on conservation of linear momentum for inviscid flow and incorporates the effect of wall friction for hydraulically smooth walls through the Chézy coefficient C which decreases with increase in wall friction. As suggested by Defina and Susin [18], the Chézy coefficient is obtained through energy balance in supercritical upstream flow from the experimentally estimated supercritical height profiles.

$$\frac{dh_{\mathrm{ver}}}{dx} = -\frac{\sin\theta + \frac{g\cos\theta}{C^2}\mathrm{Fr}^2}{\cos^2\theta(1-\mathrm{Fr}^2)}, \tag{16}$$

where h_{ver} is the vertical distance of the free surface from the conduit floor. In the case of an inclined conduit, it is different from h, the normal depth of flow defined earlier, and is the same as h for horizontal flow.

In the present experiments, $C \approx 26\,\mathrm{m}^{1/2}/\mathrm{s}$, which is much lower compared to the value used by Defina *et al.* [19] in wide open channels with hydraulically smooth walls, viz., $C \approx 65\,\mathrm{m}^{1/2}/\mathrm{s}$ for $\mathrm{Fr}_1 = 3.2{-}5.4$ and $\theta = (-0.34^\circ) - (-0.45^\circ)$. This arises due to the higher frictional resistance from the combined effect of bottom and sidewalls in narrow conduits.

The stability curve predicted from Eq. (15) is presented in Fig. 14 along with the experimental data on upslope flow. The figure shows that data points for $h_2 < H_c$ (circles) are correctly predicted as stable jumps but data sets (stars) with downstream height close to or greater than the conduit height also lie above the stability curve. This suggests that the points denoted by stars would have produced stable jumps in the absence of conduit ceiling and the new mode of instability induced by the ceiling is obviously not captured by the theoretical stability criterion [Eq. (15)]. This once again proves that the stability criteria applicable for wide open channels hold for narrow, closed conduits provided $H_c > h_2$.

VI. JUMP STABILITY AND HYSTERETIC EXCURSION IN UPSLOPE FLOW

To investigate jump stability, we perturb the stationary jump by a small change in conduit inclination and note the shift in location. When the jump changes its location but returns to the original position and stays there on withdrawal of the perturbation, it is considered stable. We

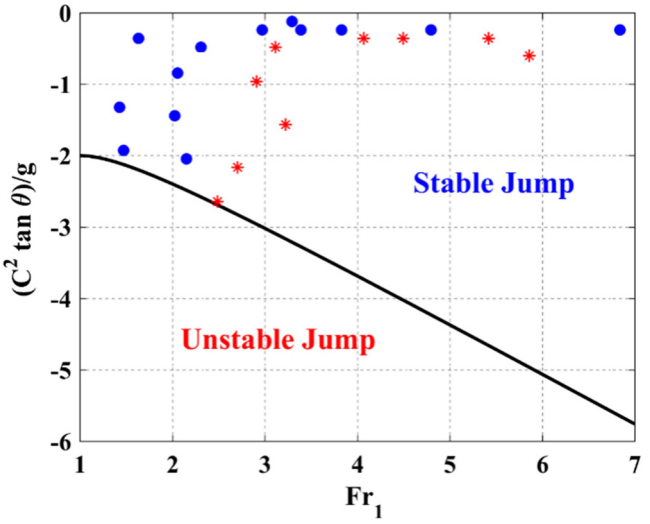

FIG. 14. Jump stability map. Stable jump domain in open channel flow lies above the curve representing Eq. (15). Circles denote stable jumps unaffected by top confinement while stars represent unstable conditions in closed conduits.

observe stable natural jumps for both upslope and downslope flow within a range of conduit inclination, referred to as the "natural" jump domain. Beyond the domain, liquid flow exhibits altogether different characteristics. For higher positive slopes, viscous drag, responsible for jump formation, is counterbalanced by the combined effect of the gravitational component along the flow direction and inertial force. This results in steady flow without a jump. In the present experiments, at the minimum flow rate, such a condition exists for $\theta \approx 1^\circ$.

On the other hand, an increase in adverse slope introduces a series of unique phenomena when the postjump liquid level is close to the conduit ceiling and triggers an altogether new hydrodynamic state. To understand, this, we consider a high water flow rate (Q_{init}) where the jump does not form within the horizontal conduit, and trace the flow evolution with gradual increase in upslope tilt. The phenomenon is pictorially depicted in Fig. 15. As the conduit is oriented at a small negative θ (upward slope) while keeping the water flow rate constant and sufficient time is allowed for flow readjustment, a hydraulic jump of low strength occurs near the exit (state 2 in Fig. 15). With a gradual increase in inclination, the jump gets stronger and moves upstream accompanied by substantial air entrainment. This trend continues with further increase in conduit inclination until the postjump free surface approaches the conduit ceiling and touches it intermittently due to local oscillations. Beyond a critical angle θ_{fb}, there is prolonged contact between liquid and conduit roof, giving rise to full bore flow after the jump. Under this condition, the jump front starts propagating upstream almost instantaneously (state 3 in Fig. 15). The movement of the jump front in a direction opposite to liquid flow resembles a bore and occurs due to the weight of liquid downstream of the jump trying to push the jump towards the inlet. Such an upstream jump propagation in upslope flow has also been reported in open channels by Baines and Whitehead [17].

We recall that full bore flow downstream of the jump is observed during horizontal flow in conduit B but since the jump is stationary, full bore flow is restricted to the downstream region only. In contrast, for the upslope conduit, countercurrent motion of the traveling jump and the liquid establishes full bore flow in the entire conduit. This not only creates a unique flow instability but also results in change of the hydrodynamic state from free surface flow with a jump to full bore flow in the entire conduit.

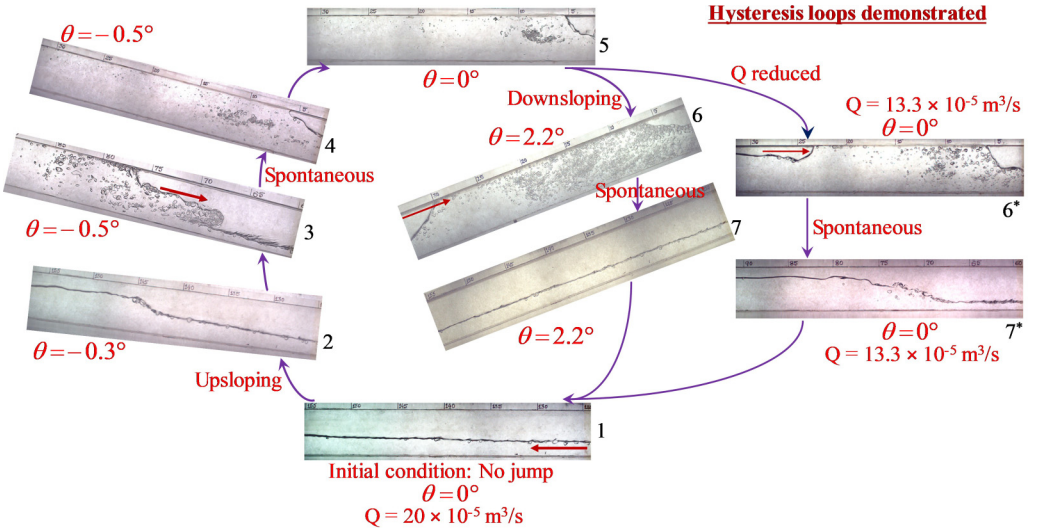

FIG. 15. Evolution of flow states through hysteresis loops 1-2-3-4-5-6-7-1 and 1-2-3-4-5-6*-7*-1.

We further note that "full bore flow" in this case cannot be reverted back to the original state by mere reversal of the conduit inclination and persists even after the conduit is restored back to the horizontal orientation. Thus Fig. 15 presents grossly different steady state hydrodynamics in state 1 and state 5. The states at identical operating conditions attained through different paths confirm unique hysteretic flow behavior.

Experiments further reveal that state 1 can be regained from state 5 by two approaches—increase in conduit tilt in the downward direction and decrease in water flow rate in the horizontal orientation. At a critical angle of downward inclination θ_{fs} the flow completely detaches from the top wall and free surface flow is established throughout the conduit. A similar phenomenon is also observed at a critical flow rate (Q_{fs}) in the horizontal orientation. In both the cases, flow detachment initiates near the conduit exit by formation of a gas finger which elongates in the upstream direction and detaches the liquid from the ceiling to reestablish free surface flow throughout the conduit. These are depicted by the sequence of flow states 1-2-3-4-5-6-7-1 and 1-2-3-4-5-6*-7*-1, respectively, in Fig. 15 with the details of the individual states listed in Table II. Interestingly, the critical angle for limiting upslope flow θ_{fb} is less than the downward critical angle θ_{fs} to resume free surface flow and the critical flow rate for complete liquid detachment from the conduit roof in horizontal flow Q_{fs} is less than Q_{init}. Figure 16 presents the two hysteresis loops in a three-parameter space, namely,

TABLE II. Specification of flow states depicted in Figs. 15 and 16.

State	θ	$Q(\text{m}^3/\text{s})$	Flow description
1	0°	20×10^{-5}	Supercritical flow: no jump
2	−0.3°	20×10^{-5}	Hydraulic jump close to conduit exit
3	−0.5°	20×10^{-5}	Downstream surface touching the top wall and the jump front propagating upstream
4	−0.5°	20×10^{-5}	Jump reaching conduit inlet
5	0°	20×10^{-5}	No change in flow configuration
6	2.2°	20×10^{-5}	Detachment of downstream surface from roof
7	2.2°	20×10^{-5}	Completely detached downstream surface: partially filled flow configuration
6*	0°	13.3×10^{-5}	Detachment of downstream surface from roof
7*	0°	13.3×10^{-5}	Downstream surface completely detached: jump assumes original appearance

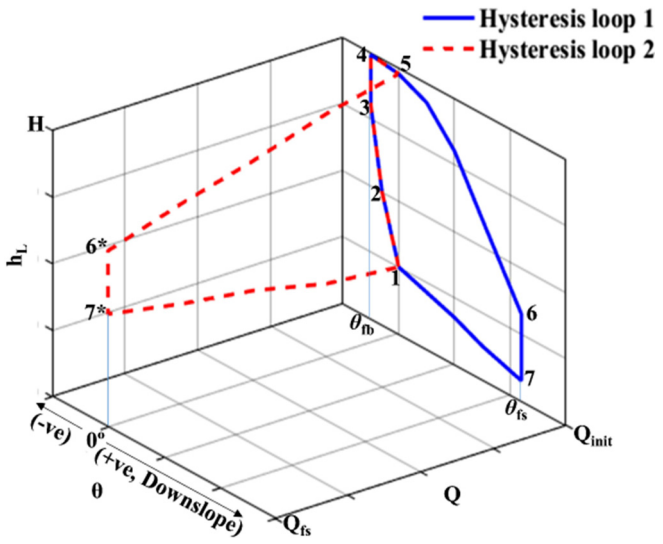

FIG. 16. Variation of liquid height averaged over conduit length with flow rate and conduit inclination.

liquid height averaged over conduit length h_L, Q, and θ. The states are denoted by the same number in both figures for convenience.

The experiments are repeated a number of times to eliminate bias in the observation. The same hysteresis phenomenon is noted each time with transition to new hydrodynamic states displayed at the same operating conditions.

We further examine the role of wetting characteristics of the conduit ceiling by repeating the experiments with the ceiling coated by the commercially available hydrophobic coating Rust-Oleum NeverWet. The contact angle for coated and uncoated acrylic plates is 148° and 62°, respectively. No qualitative difference is observed in the hysteresis phenomena when the conduit ceiling is hydrophobic. Nevertheless, some differences are observed in the critical downward angle of inclination ($\theta_{fs,sh}$) and critical flow rate ($Q_{fs,sh}$) (in horizontal conduit) at which the free surface flow is reestablished. In hysteresis loop 1, free surface flow reestablishes at a lower angle of inclination for the hydrophobic ceiling compared to an uncoated ceiling ($\theta_{fs,sh} < \theta_{fs}$) and, in hysteresis loop 2, reestablishment of free surface flow occurs at a higher flow rate ($Q_{fs,sh} > Q_{fs}$) with increase of hydrophobicity. This is expected as liquid detachment from the hydrophobic surface is relatively easier.

VII. PHASE DIAGRAM

The different hydrodynamic states observed in our experiments are caused by the coupled action of liquid flow rate and conduit inclination. Accordingly, we present the states in the Q-θ plane in Fig. 17. The phase diagram depicts the domain of natural jump bounded by conditions of full bore flow, supercritical flow, and subcritical flow throughout the conduit. Full bore flow is exhibited only under adverse ($-ve$) slope and occurs at a higher inclination angle for a higher flow rate. The zone of hysteresis is displayed in the figure as the hatched region ($H'HCI'C'H'$). Within this region, flow may either undergo natural jump or display full bore flow. From a given supercritical state if the upward slope is gradually increased until CC' is reached, natural jump occurs while if the flow rate is increased (moving along the vertical line parallel to O-O'), full bore flow persists in the hatched region. Within region $DEFGOD$, subcritical flow occurs right from the conduit inlet and liquid height increases with increase in flow rate until liquid touches the conduit ceiling at lower upslope.

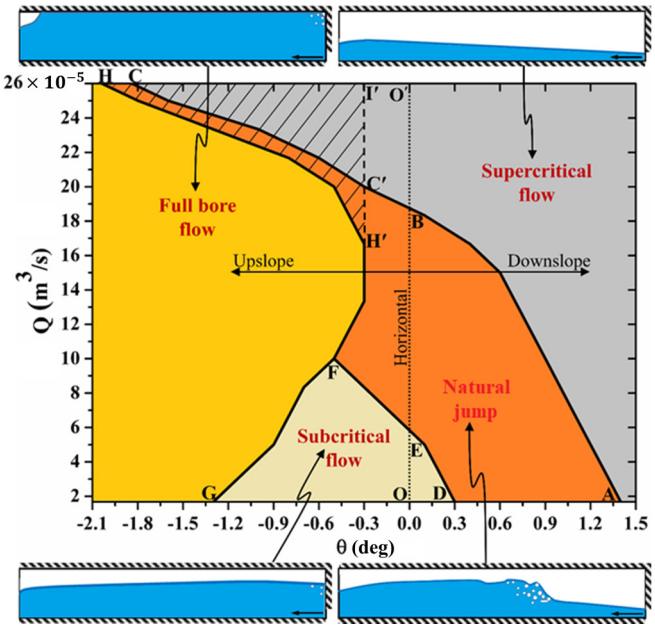

FIG. 17. Phase diagram in the Q-θ plane, depicting the hydrodynamic states observed in the present experiments.

A vertical line on the plot traces the evolution of states with change in flow rate at a constant conduit inclination, for example, line O-O' denotes the states in a horizontal conduit as a function of liquid flow rate. On increasing the velocity from very low values, supercritical flow from the inlet occurs at point E which also marks the inception of hydraulic jump in the horizontal conduit. The domain of natural jump extends from E to B. Beyond state B, the conduit length is insufficient for flow deceleration to subcritical state through viscous dissipation. As a result, natural jump does not form within the experimental range. For downward inclined conduits, the critical flow rate beyond which a jump does not form within the available conduit length is lower for a higher inclination angle and a jump may not form for high enough conduit tilts. However, in upward inclined conduits, the critical flow rate increases with θ as displayed by the shape of the boundary (curve $ABC'C$) demarcating natural jump domain from the supercritical flow region. Accordingly, the domain of natural jump shrinks substantially in upslope flows.

VIII. CONCLUSION

We explore turbulent natural jump and the associated hysteresis in narrow rectangular conduits, slightly deviated from the horizontal orientation. The complex physics under the influence of side and top wall confinement in inclined conduits is investigated through extensive experiments and theoretical analysis. The uniqueness of the study lies in (i) categorizing the emergent flow regimes as a function of conduit inclination and liquid flow rate and (ii) revealing a unique hysteretic behavior in upslope flow.

The salient conclusions can be summarized as follows:

(1) Small conduit tilt significantly influences the jump phenomena in narrow conduits, especially when the postjump height approaches the conduit ceiling.

(2) In upslope flow, once the postjump free surface touches the conduit ceiling, the jump becomes unstable and starts propagating upstream until it reaches the inlet. The stable hydrodynamic

state represented by this full bore flow can only be retraced to the original jump condition through hysteretic routes.

(3) The limiting condition for natural jump in horizontal flow (Fig. 11) is used to identify the effect of top wall confinement, and the predictions are in close agreement with the experimental observations.

(4) Shallow water theory with suitable modifications, by incorporating turbulent viscosity and coupling of lateral and vertical averaging, can be used for a reasonable prediction of turbulent natural jumps in sloping conduits. Albeit an approximate model, it provides an accurate estimation of the location and strength of the jump and the upstream free surface profiles. However, there is a consistent overprediction of the downstream free surface height. This can be attributed to the inherent simplifications of the theory which does not account for factors such as intense surface fluctuation, air entrainment into the liquid, and air entrapment between the liquid surface and the confining walls. This can be rectified by empirical tuning of the free surface height at the conduit exit.

(5) The present exercise suggests the need for a higher level numerical model or a computationally intensive CFD algorithm to capture all the relevant hydrodynamic parameters accurately. Strengthening the experimental database with conduits of different cross section and different working fluids would also be welcome.

[1] L. Rayleigh, On the theory of long waves and bores, Proc. R. Soc. London, Ser. A **90**, 324 (1914).
[2] E. J. Watson, The radial spread of a liquid jet over a horizontal plane, J. Fluid Mech. **20**, 481 (1964).
[3] S. B. Singha, J. K. Bhattacharjee, and A. K. Ray, Hydraulic jump in one-dimensional flow, Eur. Phys. J. B **48**, 417 (2005).
[4] T. Bohr, P. Dimon, and V. Putkaradze, Shallow-water approach to the circular hydraulic jump, J. Fluid Mech. **254**, 635 (1993).
[5] D. Bonn, A. Andersen, and T. Bohr, Hydraulic jumps in a channel, J. Fluid Mech. **618**, 71 (2009).
[6] J. D. Mortensen, S. L. Barfuss, and B. P. Tullis, Effects of hydraulic jump location on air entrainment in closed conduits, J. Hydraul. Res. **50**, 298 (2012).
[7] O. Pozos, C. A. Gonzalez, J. Giesecke, W. Marx, and E. A. Rodal, Air entrapped in gravity pipeline systems, J. Hydraul. Res. **48**, 338 (2010).
[8] H. Stahl and W. H. Hager, Hydraulic jump in circular pipes, Can. J. Civ. Eng. **26**, 368 (1999).
[9] V. T. Chow, *Open-Channel Hydraulics* (McGraw-Hill, New York, 1959).
[10] B. A. Bakhmeteff and A. E. Matzke, The hydraulic jump in sloped channels, Trans. Am. Soc. Mech. Eng. **60**, 111 (1938).
[11] R. W. Ellms, Hydraulic jump in sloping and horizontal flumes, Trans. Am. Soc. Mech. Eng. **54**, 113 (1932).
[12] R. W. Ellms, Computation of the tail-water depth of the hydraulic jump in sloping flumes, Trans. Am. Soc. Mech. Eng. **50**, 1 (1928).
[13] C. E. Kindsvater, The hydraulic jump in sloping channels, Trans. Am. Soc. Civ. Eng. **109**, 1107 (1944).
[14] M. Dhar, G. Das, and P. K. Das, Planar hydraulic jumps in thin film flow, J. Fluid Mech. **884**, A11 (2020).
[15] J. A. McCorquodale and M. S. Mohamed, Hydraulic jumps on adverse slopes, J. Hydraul. Res. **32**, 119 (1994).
[16] S. Pagliara and A. Peruginelli, Limiting and sill-controlled adverse-slope hydraulic jump, J. Hydraul. Eng. **126**, 847 (2000).
[17] P. G. Baines and J. A. Whitehead, On multiple states in single-layer flows, Phys. Fluids **15**, 298 (2003).
[18] A. Defina and F. M. Susin, Stability of a stationary hydraulic jump in an upward sloping channel, Phys. Fluids **15**, 3883 (2003).
[19] A. Defina, F. M. Susin, and D. P. Viero, Bed friction effects on the stability of a stationary hydraulic jump in a rectangular upward sloping channel, Phys. Fluids **20**, 036601 (2008).

[20] A. Dyment, Stability of stationary and moving hydraulic jumps in inclined conduits of arbitrary cross section, Phys. Fluids **17**, 054111 (2005).

[21] N. S. Govinda Rao and N. Ramaprasad, Application of momentum equation in the hydraulic jump, Houille Blanche **24**, 10 (1966).

[22] F. G. Carollo, V. Ferro, and V. Pampalone, Hydraulic jumps on rough beds, J. Hydraul. Eng. **133**, 989 (2007).

[23] M. Dhar, S. Ray, G. Das, and P. K. Das, Internal hydraulic jump in plane Poiseuille two-layer flow: Theoretical, numerical and experimental study, J. Fluid Mech. **912**, A45 (2021).

[24] R. P. Kate, P. K. Das, and S. Chakraborty, Hydraulic jumps due to oblique impingement of circular liquid jets on a flat horizontal surface, J. Fluid Mech. **573**, 247 (2007).

[25] M. Dhar, S. Ray, G. Das, and P. K. Das, Modulation of viscous planar jump by an obstacle in the flow path–Interrogation through shallow water equations and numerical analysis, Phys. Fluids **33**, 053609 (2021).